Peptide-Lipid Interactions of the Stress-Response Peptide TisB That Induces Bacterial Persistence

Thomas Steinbrecher,[†] Sebastian Prock,[‡] Johannes Reichert,[§] Parvesh Wadhwani,[§] Benjamin Zimpfer,[‡] Jochen Bürck,[§] Marina Berditsch,[‡] Marcus Elstner,[†] and Anne S. Ulrich[‡§*]

[†]Institute of Physical Chemistry, [‡]Institute of Organic Chemistry and Center for Functional Nanostructures; and [§]Institute of Biological Interfaces (IBG-2), Karlsruhe Institute of Technology, Karlsruhe, Germany

ABSTRACT The bacterial stress-response peptide TisB in *Escherichia coli* has been suggested to dissipate the transmembrane potential, such that the depletion of ATP levels induces the formation of dormant persister cells which can eventually form biofilms. We studied the structure and membrane interactions of TisB to find out whether it forms pores or other proton-selective channels. Circular dichroism revealed an amphiphilic α-helical structure when reconstituted in lipid vesicles, and oriented circular dichroism showed that the helix assumes a transmembrane alignment. The addition of TisB to dye-loaded vesicles caused leakage only at very high peptide concentration, notably with a Hill coefficient of 2, which suggests that dimers must be involved. Coarse-grained molecular dynamics simulations showed that membrane binding of monomeric TisB is rapid and spontaneous, and transmembrane insertion is energetically feasible. When TisB oligomers are assembled as transmembrane pores, these channels collapse during the simulations, but transmembrane dimers are found to be stable. Given the pattern of charges on the amphiphilic TisB helix, we postulate that antiparallel dimers could be assembled via a ladder of salt bridges. This electrostatic charge-zipper could enable protons to pass along a wire of trapped water molecules across the hydrophobic membrane.

INTRODUCTION

One of the major challenges in modern medicine is the fight against chronic bacterial biofilms. The main reasons for the recalcitrance of these biofilms are so-called "persister" cells. These cells, although genetically identical to ordinary bacterial cells, are in a dormant state (1). They form stochastically and show a different phenotype with high tolerance against conventional antibiotics (2) and heavy metals (3,4). Unfortunately, the mechanism of how persister cells are induced is not fully understood, making a specific treatment challenging. Moreover, it seems that persister cell formation is a highly redundant process that involves numerous genes (5,6), which makes investigations of the mechanism and a subsequent development of drugs even more complicated (7).

One way in which persisters can occur is attributed to the involvement of toxin/antitoxin (TA) systems. TA modules consist of at least two genes, where one represents the toxin and the other one serves as an antidote (8). They are found on plasmids as well as the bacterial chromosome. The free toxin usually downregulates an important cellular function, such as replication or transcription. In complex with the antitoxin, however, the toxin becomes inactivated. So far, at least 33 different TA modules have been identified in *Escherichia coli* (9), of which the HipAB system was believed to be the first one to be linked to persistence (10). HipA is a kinase which phosphorylates elongation factor Ef-Tu, which leads to a stop of translation and dormancy (11,12). There are also TA modules which get induced by the DNA damage-dependent SOS response. Among these Lex-box containing genes, the tisAB/istR1 module has been recently linked directly to persister formation (13). The toxin gene locus codes for two proteins: TisA, which does not get expressed, and the 29-amino-acid peptide TisB. The sequence

MNLVDIAILILKLIVAALQLLDAVLKYLK

is predicted to fold as an amphiphilic α-helix, as illustrated in Fig. 1. To protect *E. coli* from DNA damage under stress, TisB supposedly gets localized at the inner bacterial membrane and leads to a breakdown of the protonmotive force. The resulting depletion of cellular ATP levels then induces dormancy and the formation of drug-resistant persister cells (14).

The antitoxin istR1 is a noncoding mRNA that can form a duplex with the tisB mRNA at the ribosomal standby site, thus preventing translation of TisB (15,16). IstR1 also promotes RNase III degradation of the formed duplex (17,18). It is known that antibiotic fluoroquinones induce the SOS response, hence Dörr et al. (13) have tested the ability of different Lex-box containing mutants to form persister cells after exposure to ciprofloxacin. It turned out that tisAB mutants treated with ciprofloxacin led to a pronounced decrease in persister cell formation compared to other deletion strains. Furthermore, overexpression of TisB leads to a sharp increase in persisters, though artificial induction of the TisB expression is toxic and results in growth arrest and death in the majority of the population. These features make *tisB* an excellent candidate for

Submitted April 16, 2012, and accepted for publication July 23, 2012.

*Correspondence: anne.ulrich@kit.edu

Editor: Francesca Marassi.

0006-3495/12/10/1460/10 $2.00

http://dx.doi.org/10.1016/j.bpj.2012.07.060

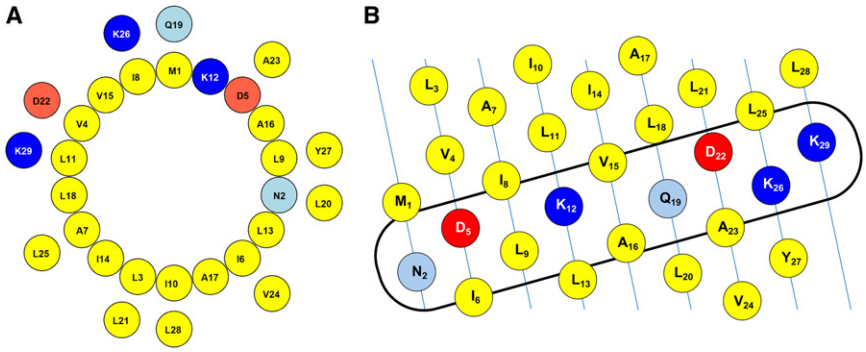

FIGURE 1 (*A*) The 29-amino-acid sequence of TisB is predicted to form an amphiphilic α-helix, as illustrated by the helical wheel plot. (*B*) The flat helix projection shows that the polar face consists of a narrow strip of predominantly charges residues. Hydrophobic side chains (*yellow*); cationic residues (*blue*); anionic residues (*red*); and polar residues (*light blue*). Figures constructed with the home-written software PROTEIN-ORIGAMI (grayscale in the print version).

a persister gene, but the molecular mode of action of the corresponding TisB peptide remains unknown.

In this study, we have investigated the structure of the stress-response peptide TisB and its interactions with bacterial model membranes. Circular dichroism (CD) was used to determine the peptide's secondary structure in lipid vesicles, and oriented CD (OCD) served to probe its alignment with respect to the membrane surface. We were also interested to find out whether and how TisB itself can lead directly to a breakdown of the pH gradient across the bacterial membrane, because the reported depletion of ATP levels is only an indirect indication of such a mode of action (14). In view of its amphiphilic character, TisB could conceivably act like many well-known amphiphilic antimicrobial peptides, which cause physical membrane perturbation and loss of cellular contents (19–22). According to the Shai-Matsuzaki-Huang model, such peptides can assemble as an oligomeric transmembrane pore (23–26), or they can permeabilize the bilayer in a transient event (27).

We have thus carried out vesicle leakage experiments to examine TisB-induced pore formation, which was extremely weak. Interestingly, the corresponding Hill coefficient of cooperativity showed that the molecular action of TisB involves dimers. To complement the experimental approach, we also performed several coarse-grained molecular dynamics (MD) simulations on TisB to examine its membrane binding and insertion into the lipid bilayer, and to compare the stability of various oligomeric transmembrane pores with the formation of parallel and antiparallel peptide dimers. Based on these combined results, we propose a comprehensive structural model and functional mechanism for TisB. A novel type of charge-zipper assembly via salt bridges can explain how the peptide could mediate the controlled passage of protons across the plasma membrane to reduce growth and protect the bacteria from stress.

MATERIALS AND METHODS

Peptide synthesis

Peptide synthesis of TisB was performed in a combined automated (first 18 amino acids (aa)) and manual (last 11 aa) approach, to optimize the yield, as described in detail in the Supporting Material. The crude peptide was purified by RP-HPLC and characterized by mass spectrometry to be >95% pure (see the Supporting Material for more details). The antimicrobial peptides Alamethicin, PGLa, and Magainin-2 were synthesized as described previously (21,28,29).

CD samples

These were prepared by cosolubilizing TisB at a peptide/lipid ratio (mol/mol) of 1:100 with dimyristoylphosphatidylcholine (DMPC) in chloroform/methanol 1/1 (v/v), or with dioleoylphosphatidylcholine (DOPC) in pure methanol (see the Supporting Material for more details). After drying, the peptide/lipid film was dispersed in phosphate buffer (10 mM, pH 7) and homogenized. Small unilamellar vesicles (SUVs) for conventional CD analysis were generated by sonication. Oriented CD samples were prepared from the SUV dispersions on a quartz glass plate, as previously described in Bürck et al. (30). CD measurements of SUV were recorded on a J-815 spectropolarimeter (JASCO, Groß-Umstadt, Germany) between 260 and 185 nm at 0.1-nm intervals using 1-mm quartz-glass cells (Suprasil; Hellma USA, Plainview, NY) at 30°C. To calculate mean residue ellipticities, the concentration of the TisB stock was determined by UV absorbance at 280 nm. For oriented CD analysis, an OCD cell was used that had been developed and built in-house (30). Eight spectra were acquired at different sample rotations to average-out linear dichroism effects, and the lipid background was subtracted, as suggested in Wu et al. (31), Olah and Huang (32), and Chen et al. (33).

Dye leakage experiments

Dye leakage experiments were performed on large unilamellar DOPC vesicles (LUVs), prepared by extrusion (Avanti Mini Extruder; Avanti Polar Lipids, Alabaster, AL) through a polycarbonate filter with 100-nm pores, in the presence of dye and quencher (12.5 mM 8-aminonaphthalene-1,3,6-trisulfonic acid (ANTS), 45 mM p-xylene-bis-pyrimidinium bromide (DPX), 53 mM NaCl, 10 mM Na-phosphate, pH 7.5). The LUVs were washed on Sephacryl 100-HR (Sigma, St. Louis, MO). Leakage experiments were carried out on a FluoroMax2 spectrofluorimeter (HORIBA Jobin Yvon, Unterhaching, Germany) by measuring the fluorescence dequenching resulting from the efflux of the entrapped fluorophore/quencher pair ANTS/DPX with excitation set at 422 nm (6 nm slit) and emission at 515 nm (6 nm slit) (34). The final lipid concentration was 200 μM, the temperature was 30°C, and TisB and the other peptides were added from a 500-μM methanolic stock solution. After 30 min, 0.5 vol % Triton-X100 was added to solubilize the vesicles and to yield the 100% leakage level.

MD simulations

Molecular dynamics (MD) simulations were performed with the MARTINI force field (35,36), optimized for the description of peptides and proteins

(37,38). In this coarse-grained approach, approximately four heavy atoms plus bound hydrogens are combined into a single bead. Simulations were conducted using Ver. 4.5.3 of the GROMACS program (39–41). The systems were set up using 800 DMPC lipid molecules and 8000 water particles forming a 155 × 155 Å^2 bilayer. The TisB peptide was built as an idealized α-helix using the leap module of the AmberTools modeling suite, and transformed into the CG representation using the *atom2cg* tool (42,43). Simulations were typically conducted using 1 ns of equilibration, followed by 120 ns of production simulations, unless indicated otherwise in the text. Visualization used VMD version 1.8.6 (44,45), molecule images were rendered in POV-Ray 3.6.1 (46). Free energy calculations were conducted using the umbrella sampling formalism (47–49) (see the Supporting Material for more details).

RESULTS AND DISCUSSION

Circular dichroism of membrane-bound TisB

Conventional CD is a well-established technique for secondary structure analysis of proteins and peptides in aqueous solution (50) as well as in lipid environment (51–53). We reconstituted TisB at a peptide-to-lipid (P/L) ratio of 1:100 (mol/mol) in small unilamellar vesicles of DMPC or DOPC in aqueous suspension, at a temperature of 30°C where the lipid is in the fluid phase. The corresponding CD spectra in Fig. 2 *A* show a positive band at 193 nm and two negative bands at 209 and 222 nm, which is the characteristic signature of an α-helical fold. The secondary structure composition of membrane-bound TisB was quantitatively determined using three different deconvolution algorithms provided at DICHROWEB (54,55). All three algorithms give consistent results (see Table S1 in the Supporting Material), with an α-helical percentage of 74–80%, and only minor fractions of unordered or β-strand/β-turn conformation. These data are in fairly good agreement with results obtained from secondary structure prediction programs AGADIR (56) and GOR IV (57), which calculate a helicity of 77% and 69%, respectively. The percentage determined from the CD experiment corresponds to ~22 out of the 29 amino acids, which matches well with the typical length of a protein transmembrane segment. CD structural analysis in lipid vesicles thus confirms that TisB assumes a predominantly helical conformation, both in DMPC and DOPC.

When applied to macroscopically oriented lipid bilayer samples, oriented CD (OCD) spectroscopy can reveal the alignment of α-helical peptides with respect to the membrane normal (30–32,51,52,58). Different characteristic helix alignments can be clearly distinguished, such as surface-bound, obliquely tilted, or transmembrane-inserted. The relative intensity of the negative "fingerprint" band around 208 nm is directly indicative of the helix tilt angle. When the 208-nm band is more negative than the 222-nm band this indicates a helix alignment in the plane of the lipid layer, whereas zero or even positive intensity at 208 nm indicates an upright transmembrane helix. When TisB was reconstituted in oriented DMPC bilayers with P/L = 1:100, scattering artifacts led to a poor quality of the spectra, as previously observed also with other peptides (59). In DOPC, on the other hand, the same OCD lineshape was obtained with much better quality as seen in Fig. 2 *B*. The complete absence of the 208-nm band suggests that the TisB helix is aligned in a transmembrane state. In view of the charged residues Asp^5, Lys^{12}, Asp^{22}, and Lys^{26} on the polar face of the helix (Fig. 1), this orientation implies that TisB must be assembled in some kind of oligomeric structure in the hydrophobic bilayer environment.

TisB-induced dye leakage from large unilamellar vesicles

Many amphiphilic helical peptides perturb lipid vesicles by forming pores or complete micellarization, which can be conveniently characterized by fluorescent dye release experiments (34). The time course of peptide-induced leakage is monitored by ANTS/DPX dequenching. Here, we compared the membrane-perturbing effect of TisB with that of the well-known antimicrobial peptaibol Alamethicin, and with a 1:1 molar mixture of the antimicrobial peptides PGLa and Magainin. The hydrophobic Alamethicin is generally assumed to assemble as an oligomeric barrel-stave pore (28,61), whereas PGLa/Magainin is supposed to synergistically form a long-lived toroidal wormhole in the lipid bilayer (21,24,62). As a control, we used the pH-uncoupler CCCP, which is known to break down membrane potential

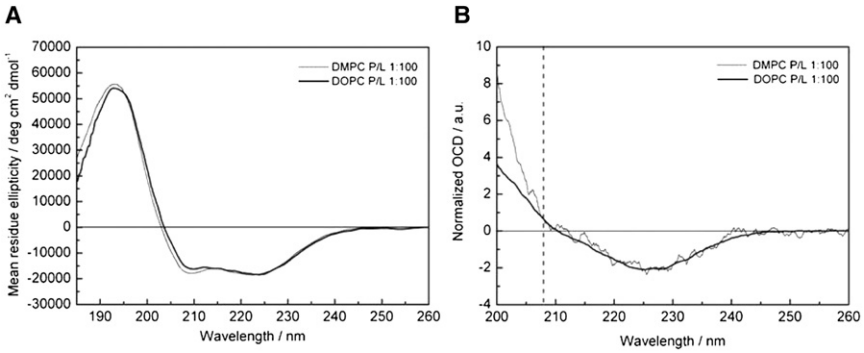

FIGURE 2 (*A*) CD spectrum of TisB in DMPC and DOPC liposomes, showing a characteristic α-helical lineshape. (*B*) Oriented CD spectra of TisB in macroscopically oriented DMPC and DOPC bilayers reveals that the helix is aligned in a transmembrane state. Signals are only shown down to 200 nm due to poor signal/noise below this wavelength, which is attributed to the olefinic bands in DOPC. TisB was only poorly reconstituted in DMPC, and peptide aggregation in the membrane lead to scattering artifacts and reduced spectral intensity. The spectrum in DMPC was blown-up to the ellipticity value at 224 nm of the spectrum in DOPC to illustrate the similarity in the lineshapes of both samples.

by acting as a selective proton shuttle. Fig. 3 *A* illustrates the time course of the experiments.

After establishing the initial fluorescence intensity level as 0% leakage, the respective compounds were added to large unilamellar DOPC vesicles at a P/L ratio (molecule/lipid) of 1:50. (Note that DMPC vesicles would have been difficult to prepare for leakage experiments due to their lipid phase transition at room temperature.) After 30 min, the vesicles were solubilized by 0.5 vol% Triton X-100 to define the 100% leakage level. Almost no effect is seen for TisB and CCCP, whereas the antimicrobial peptides induce dramatic dye release. The pore-forming Alamethicin and PGLa/Magainin lead to rapid and complete leakage within a few seconds, whereas TisB and CCCP show no significant effect. Quantitative analysis gave 100% leakage for the antimicrobial peptides, but only 4.6% for TisB, and 1.1% for CCCP.

These findings clearly indicate that TisB does not cause significant membrane perturbation at an ambient concentration of 4 μM, in contrast to typical pore-forming peptides. It is unlikely that this low activity is due to a lack of binding, because

1. TisB has an exposed hydrophobic surface area close to that of Alamethicin and PGLa/Mag,
2. electrostatic interactions do not (dis-)favor any of the peptides in the zwitterionic DOPC vesicles, and
3. the MD simulations below show a rapid and spontaneous membrane insertion in DMPC.

Nevertheless, our results seem to contrast a preliminary report by Gurnev et al. (63), who found that TisB concentrations higher than 10 μM induce multilevel conductive states in black lipid membranes, resembling pore formation by Alamethicin. We therefore increased the TisB concentration in a systematic series of leakage experiments, and we indeed observed almost 40% leakage at 40 μM concentration. However, leakage under those conditions is not surprising, because any amphiphilic compound with a high membrane affinity is likely to cause nonspecific disruption of the bilayer at such an unphysiologically high peptide/lipid ratio of 1:5. The most remarkable finding of our concentration-dependent series of leakage experiments, however, is the Hill coefficient of 1.93 $\pm$ 0.07 with a correlation coefficient of $R^2 = 0.99551$, shown in Fig. 3 *B*. The Hill coefficient describes the number of molecules that are cooperatively engaged in a concerted process such as pore formation. As this number comes very close to two, our results indicate that the active unit of TisB causing leakage must be a dimer.

Coarse-grained MD simulations show spontaneous binding of TisB to the lipid bilayer

To study the tendency of TisB to spontaneously bind to lipid bilayers, we performed a series of coarse-grained MD simulations (see the Supporting Material for details). A single helical peptide was placed parallel to the surface of a pre-equilibrated DMPC lipid bilayer with 30 Å separation. The system was subjected to a standard equilibration protocol of 500 steps of steepest-descent minimization, followed by 3 ns temperature and density equilibration with harmonic restraints on the peptide. During 120 ns of unrestrained MD simulation, the C-terminus started interacting with the bilayer surface after 1 ns, followed by a complete binding of the peptide to the bilayer.

A visualization of this process is provided in Movie S1 in the Supporting Material. It shows that after ~10 ns, the helix had embedded itself flat within the bilayer and began to diffuse in the two-dimensional plane of the membrane. There, it maintained its geometry of lying parallel slightly below the bilayer surface, with the charged side chains oriented toward the aqueous solvent. A particle density profile plot of this resulting TisB/DMPC system is shown in Fig. 4 *A*. During the binding process the peptide turned from its initial alignment parallel above the bilayer, by almost 90° for the initial bilayer contact, and then rotated back to eventually lie parallel below the bilayer surface. The simulation was repeated several times with slightly different starting geometries, always leading to rapid bilayer insertion of the helical peptide. Repeating the simulations of the insertion process with two peptides simultaneously

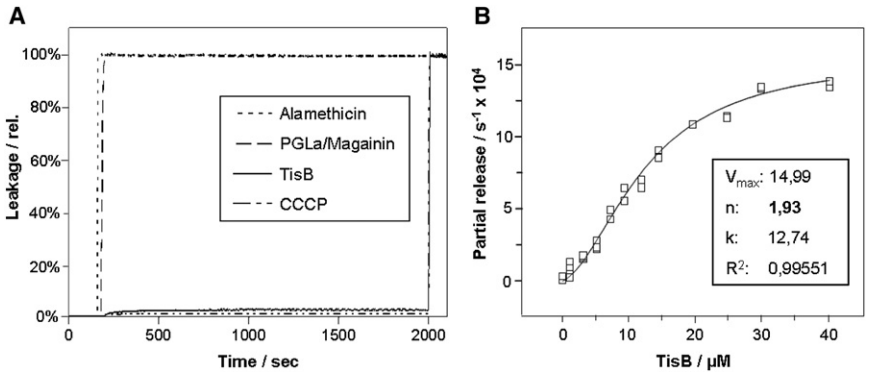

FIGURE 3 (*A*) Time course of peptide-induced leakage of the fluorophore ANTS from large unilamellar DOPC vesicles. TisB and the pH-uncoupler CCCP induce essentially no leakage, whereas the typical pore-forming peptides Alamethicin and PGLa/Magainin cause complete leakage within seconds. The P/L ratio of 1:50 corresponds to 4 μM peptide or CCCP in the presence of 200 μM lipid (135 mM NaCl, 10 mM Na-phosphate, pH 7.5, 30°C). (*B*) Concentration-dependent leakage monitored by the initial dye release, determined by the slope of the increasing fluorescence within the first 20 s. The data were fitted to $V(c) = V_{max} \times [c^n/(k^n+c^n)]$ to obtain a Hill coefficient of 1.93 $\pm$ 0.07, which indicates that TisB is active as a dimer.

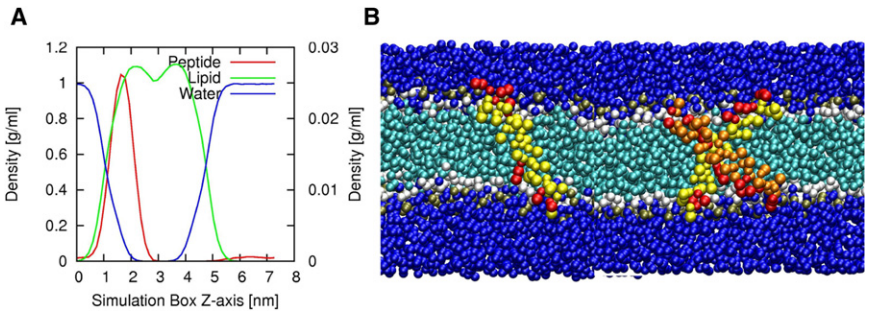

FIGURE 4 (*A*) Average particle density profile from a 120-ns coarse-grained MD simulations of bilayer embedded TisB. The peptide lies parallel to the bilayer surface, about 0.5 nm above the central lipid density peak. In this position, the amphiphilic TisB helix can engage in favorable interactions with water and with hydrophobic lipid acyl chains. Note the different scale of the density axis used for the peptide (*right side*) and the rest of the system (*left*). (*B*) Coarse-grained molecular dynamics simulations of the TisB helix tilt of an equilibrated monomer (*left*) and dimer (*right*) in a DMPC bilayer, starting from an upright transmembrane alignment. The peptides uniformly adopt a tilt angle of about 40° with respect to the bilayer-normal, and in the dimer the peptides adopt a crossing angle of almost 90°. The dimer displayed is formed from antiparallel peptides. Note that all charged peptide groups (*red beads*) are situated at or very close to the bilayer surface, i.e., they are snorkeling. Water (*blue*); lipid headgroups (*white/gray*); and tails (*cyan*). Peptides (*yellow* or *orange*); charged peptide residues (*red*). Not all solvent and lipid molecules are displayed for clarity (grayscale in the print version).

showed no evidence of dimer formation for the peptide in the surface-bound state.

Stability of TisB in a transmembrane alignment

From the OCD analysis, we know that TisB can assume a stable transmembrane alignment in liquid crystalline DMPC. To test the stability and oligomerization tendencies of TisB by coarse-grained MD simulations, we constructed various starting geometries:

1. a single bilayer-spanning peptide,
2. parallel dimers,
3. antiparallel dimers,
4. parallel tetramers, and
5. antiparallel tetramers.

The peptides were placed into preequilibrated solvated bilayers of 800 DMPC molecules. All peptide helices were aligned to the z axis, parallel to the bilayer-normal. For oligomers, peptides were rotated such that their polar groups were facing each other at 20 Å center-of-mass separation. Initial bad contacts between peptides and environment were corrected by removing all lipid and solvent molecules for which >50% of particles lay within 0.5 nm of a peptide bead. This was followed by a removal of sterical clashes, by moving all remaining lipid particles within 0.5 nm of a peptide bead along a vector in the xy plane pointing away from the peptide center of mass. All models were subjected to an equilibration procedure consisting of 500 steps of steepest-descent minimization, and 0.5 ns temperature equilibration with strong positional restraints on the peptides to allow for solvent and lipid packing. After 0.5 ns final unrestrained equilibration, all models were simulated for 120 ns of free dynamics.

All peptides, regardless of their oligomerization state, remained in a transmembrane alignment. No peptide became oriented parallel to the bilayer surface or was released from it. All helices adopted a tilt angle of ~40° with respect to the bilayer-normal, which remained relatively constant over the whole simulation length with an average standard deviation of 8°. These findings are fully compatible with the helix alignment determined experimentally by OCD. All dimers and tetramers remained densely packed together, with peptide center-of-mass distances of ~1.2 nm. The dimers maintained contact mostly via residues 10–19 along the central stretch of the peptide, with the helix axes tilted against each other at crossing angles close to 90°.

In the case of the antiparallel tetramer, the formation of two antiparallel dimers with their polar groups pointing toward each other was observed, with both dimers in contact with one another. The charged groups of the amphiphilic peptides tend to orient toward or into the bilayer surface and solvent. This snorkeling behavior helps to stabilize the charged groups in membrane complexes. Fig. 4 *B* illustrates some typical peptide geometries, and the calculated structural data are summarized in Table S2. These results suggest that TisB, both as a monomer and as various oligomers, can adopt a stable transmembrane alignment in the bilayer, though no spontaneous transitions to the surface-bound state were found. This means that neither a breakup of peptide clusters within the bilayer, nor a realignment toward the membrane surface, occur within the timescale of the simulation.

Instability of oligomeric transmembrane pores

Another conceivable way for the amphiphilic TisB helix to insert into lipid bilayers is via assembly into discrete oligomeric pores, similar to the well-known antimicrobial peptides Alamethicin and PGLa/Magainin (21,24,28,33,64). Because the timescale of spontaneous pore formation can lie significantly above the accessible simulation times we decided to test the stability of preformed oligomeric pores in a solvated DMPC lipid bilayer. Pores were built by placing symmetric rings of 8, 12, 16, or 18 peptides into a preequilibrated bilayer of 800 DMPC molecules solvated with ~8000 CG water molecules. Both parallel and antiparallel peptide assemblies were constructed either with all C-termini on the same side of the bilayer, or with alternating alignments. The initial pore diameters were set to 3.6, 5.2,

7.0, and 8.0 nm for the 8-, 12-, 16-, and 18-mers, respectively. All lipid and solvent molecules inside the pore were removed, and sterical overlap was avoided as described above. By constructing the pore systems using the *inflategro* method (65), similar starting geometries were obtained with slightly deformed lipid bilayers.

The pore models were equilibrated as above, and the central channel of the pores spontaneously filled with water during equilibration. Then all pore models were simulated for 1.2 μs of free dynamics. During this time, the architecture of the peptide oligomers and the number of water molecules in the channels was monitored. The number of water molecules in the pores decreased rapidly. For example, the four largest pores (parallel and antiparallel 16-mers and 18-mers) contained, on average, 131 solvent particles after 120 ns, but only 49 solvent particles after 240 ns. The movement of water out of the central channels was accompanied by structural deformations of the pore walls, as illustrated in Fig. 5. After 1.2 μs simulation time, all pore models had deformed into seemingly random peptide assemblies in the bilayer, without any continuous thread of solvent spanning the bilayer. The only exception was the case of the antiparallel 12-mer, for which a thin water channel persisted longer, but also disappeared after 5.5 μs. In no case did a ruptured solvent channel reform in these simulations.

When the peptide pores collapsed, the oligomeric clusters remained in a transmembrane alignment and did not separate into smaller oligomers nor release any monomers laterally. These findings indicate that TisB has no tendency to form oligomeric pores in a lipid bilayer. Instead, the peptides tend to cluster laterally, possibly due to hydrophobic mismatch in the comparatively thin DMPC bilayer. These findings fully support our leakage experiments above, which had shown that TisB does not permeabilize the membrane at ambient concentration, in contrast to the pore-forming antimicrobial peptides Alamethicin and PGLa/Magainin.

Free energies of peptide-lipid interactions

To obtain a more-quantitative picture of TisB membrane insertion, we conducted free-energy umbrella-sampling MD simulations. Various conceivable insertion and oligomerization processes were examined, such as horizontal and vertical bilayer insertion, and dimerization of TisB in either of these two states. (Please consult the Supporting Material for details, where the potential of mean force curves are shown as Fig. S3, *A–D*.) From these simulations

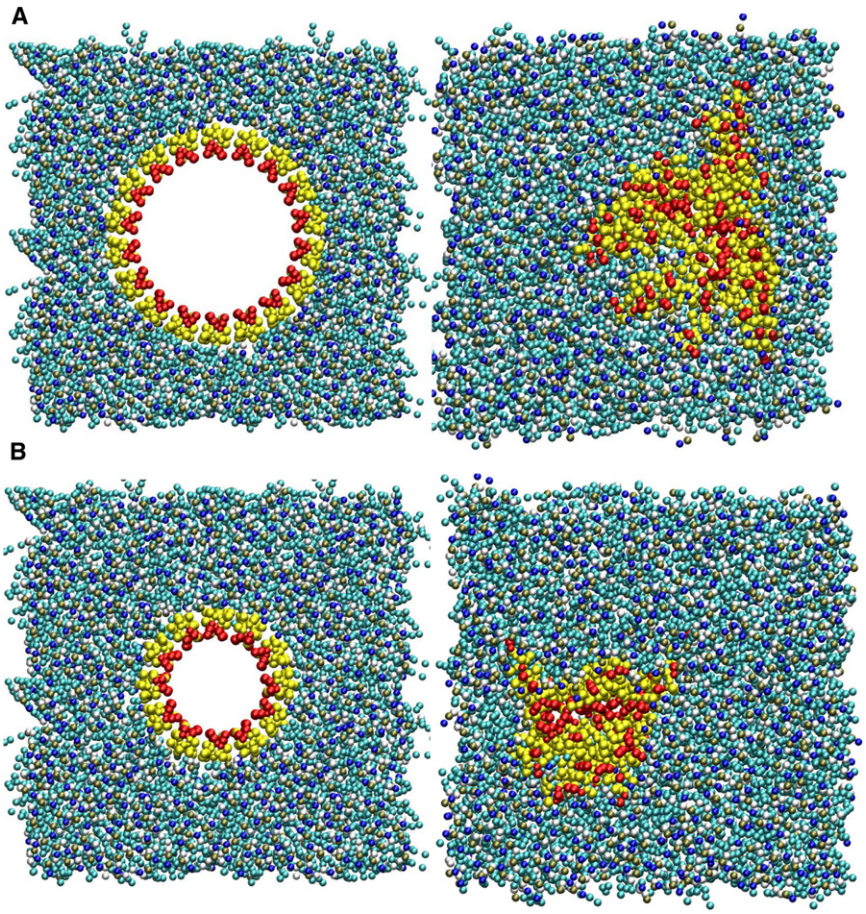

FIGURE 5 (*A* and *B*) Oligomeric transmembrane pores of TisB in a DMPC bilayer are not stable during unrestrained MD simulations. Depicted are the starting geometries for an octadecameric pore built from parallel helices (*top*), and for a dodecameric pore built from antiparallel helices (*bottom*). For the 18-mer, the pore collapsed over a 1.2 microsecond simulation, while for the 12-mer the central water channel disappeared after 5.5 microseconds. (*Bead representation*) Peptides; polar residues (*red*), and nonpolar residues (*yellow*). The lipid bilayer is seen from the top; solvent particles are not shown (grayscale in the print version).

a comprehensive picture emerges, in which a TisB peptide binds rapidly to the membrane in a surface-bound state. An activation barrier has to be overcome when the surface-bound peptide realigns into a transmembrane state, but the free energy curves show that this process is energetically feasible. A subsequent dimerization of two transmembrane-inserted peptides is then predicted to be rapid and spontaneous. The overall sequence of events gives a reasonable impression of how transmembrane TisB dimers could be formed in vivo. Notably, our umbrella-sampling simulations indicate that transmembrane dimers of TisB can indeed form and remain stable.

CONCLUSIONS

Starting from secondary structure predictions and implicit microbiological observations, our combined experimental spectroscopic and MD simulation studies have provided a first, to our knowledge, working model for the structure and function of the biofilm-inducing stress-response peptide TisB from *E. coli*. The expected amphiphilic α-helical structure of the 29-aa peptide was confirmed by CD, and OCD showed that the helix assumes a stable transmembrane alignment in DMPC and DOPC bilayers. Fluorescence dequenching experiments indicated that TisB does not induce any significant leakage in uncharged lipid vesicles at ambient concentration, unlike the representative pore-forming antimicrobial peptides Alamethicin and PGLa/Magainin. Only at very high peptide/lipid ratios did we observe significant membrane perturbations, notably with a Hill coefficient of 2, suggesting that dimers are the active unit of TisB.

A coarse-grained molecular mechanics model allowed rapid analysis of peptide-lipid and peptide-peptide interactions, yielding free energies for several structural processes summarized in Fig. S3. The amphiphilic helical peptide spontaneously binds flat to the bilayer surface. Realignment into the transmembrane state is possible, though considerable free energy barriers have to be overcome. Several intermediate stages between surface-bound and fully inserted alignments are conceivable, differing by the number of charged side chains that have crossed the hydrophobic bilayer core. Once in the transmembrane state, the TisB monomers can spontaneously assemble as stable dimers. Oligomeric barrel-shaped or toroidal pores, on the other hand, are not stable in long coarse-grained MD simulations and collapse into peptide clusters.

Now the question arises, whether and how the transmembrane TisB dimers can mediate the passage of protons across the hydrophobic lipid bilayer. MD simulations suggest that both parallel and antiparallel dimers have a similar stability. Inspection of the side-chain arrangements in the flat helix projection of Fig. 1 *B* suggests, however, that the antiparallel head-to-tail assembly could be the preferred form. The four charged side-chains Asp^{5}, Lys^{12}, Asp^{22}, and Lys^{26} lie on a narrow strip along the polar face of the helix, with an alternating pattern of positive and negative charges. It is tempting to speculate that two transmembrane helices could assemble as a coiled-coil and form four intermolecular salt bridges in the antiparallel arrangement, as illustrated in Fig. 6.

The resulting row of salt bridges would thus act like an electrostatic charge-zipper and hold the TisB dimer together, similar to our recent observation on the TatA protein (T.H. Walther, C. Gottselig, S.L. Grage, M. Wolf, A.V. Vargiu, M.J. Klein, S.Volmer, S. Prock, M. Hartmann, S. Afonin, E. Stockwald, H. Heinzmann, W. Wenzel, P. Ruggerone, and A.S. Ulrich, unpublished). The immersion of charged residues into membranes has often been considered unfavorable in the past (66), but more recent analyses have shown that buried salt bridges in globular proteins tend to make a stabilizing contribution (67). The energetic penalty of dehydration is paid off favorably by hydrogen-bonding and electrostatics. In TisB, the possibility to mutually

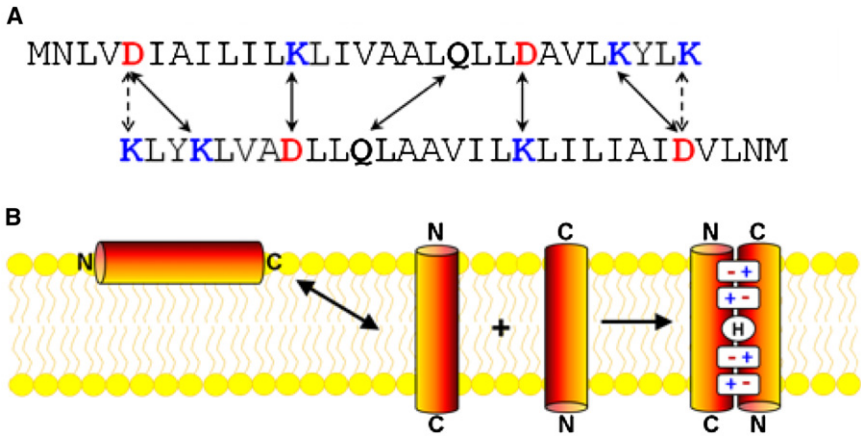

FIGURE 6 (*A*) Postulated intermolecular salt bridges in an antiparallel TisB dimer, and hydrogen-bonding interaction between the central Gln^{19} residues. (*B*) Schematic overview of the interaction of TisB with lipid bilayers, and of the hypothetical peptide-peptide interactions leading to functionally active dimers. After binding to the membrane surface, the helical peptide can flip into a transmembrane alignment with either its N-terminus or its C-terminus first. After this two-state equilibrium, the transmembrane peptides immediately dimerize. The most favorable form is proposed to be an antiparallel dimer, as it could be stabilized by a row of four intermolecular salt bridges and the central Gln^{19} (indicated as the *central circled* "*H*"). This polar interface could allow protons to selectively move across the lipid bilayer by means of a Grotthuss mechanism along a wire of water molecules, or it could support the direct passage of a hydronium ion.

compensate eight charges would strongly reduce the energetic cost of placing them in the low dielectric environment of the lipid bilayer.

As of this writing, the coarse-grained model is unable to provide enough information on such subtle interactions, which depend strongly on the exact positions and torsion angles of the side chains. During the peptide insertion studies, we had noted the formation of intramolecular salt bridges and some clusters of solvent molecules around the membrane immersed charged side chains, but these may well be artifacts of the coarse-grained simulation model. Especially the uniform dielectric constant employed in these simulations makes the movement of charges into regions of lower polarity too easy. Therefore, follow-up, fully atomistic MD simulations of the membrane system should now be employed to study the proposed TisB complexes in more detail.

As a working hypothesis, we may propose a model for the molecular mechanism of TisB and its ability to selectively carry protons across the lipid bilayer. Based on the idea that the antiparallel dimer is stabilized by an electrostatic charge zipper, it is conceivable that some water molecules are trapped along the ladder of salt bridges. Notably, located right at the center of this pathway there is residue Gln^{19} (see Fig. 1 *B* and Fig. 6). This side chain would be an ideal hydrogen-bonding partner to form yet another intermolecular bridge between the two TisB monomers, which might act as a gate. Single protons could thus cross the lipid bilayer, by one of two methods: 1) traveling along a wire of water molecules by means of a Grotthuss mechanism; or 2), a hydronium ion could travel along the polar dimer interface (68). Either process would dissipate the protonmotive force across the membrane, which is needed by the bacterium for respiration and ATP production. The concentration of TisB is obviously strictly controlled by the antitoxin istR1, which allows the expression of TisB only in response to stress. By decreasing the transmembrane potential in such a controlled manner, *E. coli* can regulate and shut down its metabolism to enter the dormant state. When the stress is over, the undamaged persister cells will start to grow as biofilms, i.e., a different phenotype with a newly acquired high tolerance against drugs and heavy metals.

If our structural working hypothesis turns out to be correct, TisB appears to represent the smallest selective ion channel encountered so far. The idea of an electrostatic charge-zipper is a novel concept, to our knowledge, that may be able to describe a new type of protein-protein interaction in membranes.

SUPPORTING MATERIAL

Two figures, two tables, additional Materials and Methods, one movie, and references (69–80) are available at http://www.biophysj.org/biophysj/supplemental/S0006-3495(12)00983-6.

We acknowledge financial support from the Deutsche Forschungsgemeinschaft Center for Functional Nanostructures (TP E1-2 and E1-6).

REFERENCES

1. Dawson, C. C., C. Intapa, and M. A. Jabra-Rizk. 2011. "Persisters": survival at the cellular level. *PLoS Pathog.* 7:e1002121.
2. Balaban, N. Q., J. Merrin, …, S. Leibler. 2004. Bacterial persistence as a phenotypic switch. *Science.* 305:1622–1625.
3. Harrison, J. J., H. Ceri, …, R. J. Turner. 2005. Persister cells mediate tolerance to metal oxyanions in *Escherichia coli*. *Microbiology.* 151: 3181–3195.
4. Harrison, J. J., R. J. Turner, and H. Ceri. 2005. Persister cells, the biofilm matrix and tolerance to metal cations in biofilm and planktonic *Pseudomonas aeruginosa*. *Environ. Microbiol.* 7:981–994.
5. Hansen, S., K. Lewis, and M. Vulić. 2008. Role of global regulators and nucleotide metabolism in antibiotic tolerance in *Escherichia coli*. *Antimicrob. Agents Chemother.* 52:2718–2726.
6. Vázquez-Laslop, N., H. Lee, and A. A. Neyfakh. 2006. Increased persistence in *Escherichia coli* caused by controlled expression of toxins or other unrelated proteins. *J. Bacteriol.* 188:3494–3497.
7. Lewis, K. 2010. Persister cells. *Annu. Rev. Microbiol.* 64:357–372.
8. Hayes, F. 2003. Toxins-antitoxins: plasmid maintenance, programmed cell death, and cell cycle arrest. *Science.* 301:1496–1499.
9. Yamaguchi, Y., J. H. Park, and M. Inouye. 2011. Toxin-antitoxin systems in bacteria and archaea. *Annu. Rev. Genet.* 45:61–79.
10. Moyed, H. S., and S. H. Broderick. 1986. Molecular cloning and expression of HipA, a gene of *Escherichia coli* K-12 that affects frequency of persistence after inhibition of murein synthesis. *J. Bacteriol.* 166: 399–403.
11. Correia, F. F., A. D'Onofrio, …, K. Lewis. 2006. Kinase activity of overexpressed HipA is required for growth arrest and multidrug tolerance in *Escherichia coli*. *J. Bacteriol.* 188:8360–8367.
12. Schumacher, M. A., K. M. Piro, …, R. G. Brennan. 2009. Molecular mechanisms of HipA-mediated multidrug tolerance and its neutralization by HipB. *Science.* 323:396–401.
13. Dörr, T., M. Vulić, and K. Lewis. 2010. Ciprofloxacin causes persister formation by inducing the TisB toxin in *Escherichia coli*. *PLoS Biol.* 8:e1000317.
14. Unoson, C., and E. G. H. Wagner. 2008. A small SOS-induced toxin is targeted against the inner membrane in *Escherichia coli*. *Mol. Microbiol.* 70:258–270.
15. Vogel, J., L. Argaman, …, S. Altuvia. 2004. The small RNA IstR inhibits synthesis of an SOS-induced toxic peptide. *Curr. Biol.* 14: 2271–2276.
16. Darfeuille, F., C. Unoson, …, E. G. Wagner. 2007. An antisense RNA inhibits translation by competing with standby ribosomes. *Mol. Cell.* 26:381–392.
17. Weel-Sneve, R., M. Bjørås, and K. I. Kristiansen. 2008. Overexpression of the LexA-regulated tisAB RNA in *E. coli* inhibits SOS functions; implications for regulation of the SOS response. *Nucleic Acids Res.* 36:6249–6259.
18. Sharma, C. M., and J. Vogel. 2009. Experimental approaches for the discovery and characterization of regulatory small RNA. *Curr. Opin. Microbiol.* 12:536–546.
19. Grage, S. L., S. Afonin, and A. S. Ulrich. 2010. Dynamic transitions of membrane-active peptides. *In* Methods in Molecular Biology. A. Giuliani and A. C. Rinaldi, editors. 183–207.
20. Afonin, S., S. L. Grage, …, A. S. Ulrich. 2008. Temperature-dependent transmembrane insertion of the amphiphilic peptide PGLa in lipid bilayers observed by solid state ^{19}F NMR spectroscopy. *J. Am. Chem. Soc.* 130:16512–16514.

21. Tremouilhac, P., E. Strandberg, …, A. S. Ulrich. 2006. Synergistic transmembrane alignment of the antimicrobial heterodimer PGLa/magainin. *J. Biol. Chem.* 281:32089–32094.

22. Hartmann, M., M. Berditsch, …, A. S. Ulrich. 2010. Damage of the bacterial cell envelope by antimicrobial peptides gramicidin S and PGLa as revealed by transmission and scanning electron microscopy. *Antimicrob. Agents Chemother.* 54:3132–3142.

23. Matsuzaki, K. 1999. Why and how are peptide-lipid interactions utilized for self-defense? Magainins and tachyplesins as archetypes. *Biochim. Biophys. Acta.* 1462:1–10.

24. Shai, Y. 1999. Mechanism of the binding, insertion and destabilization of phospholipid bilayer membranes by α-helical antimicrobial and cell non-selective membrane-lytic peptides. *Biochim. Biophys. Acta.* 1462: 55–70.

25. Yang, L., T. M. Weiss, …, H. W. Huang. 2000. Crystallization of antimicrobial pores in membranes: magainin and protegrin. *Biophys. J.* 79:2002–2009.

26. Afonin, S., U. H. N. Dürr, …, A. S. Ulrich. 2008. Solid state NMR structure analysis of the antimicrobial peptide Gramicidin S in lipid membranes: concentration-dependent re-alignment and self-assembly as a β-barrel. *In* Current Topics in Chemistry. T. Peters, editor. 139–154.

27. Ieronimo, M., S. Afonin, …, A. S. Ulrich. 2010. ^{19}F NMR analysis of the antimicrobial peptide PGLa bound to native cell membranes from bacterial protoplasts and human erythrocytes. *J. Am. Chem. Soc.* 132:8822–8824.

28. Maisch, D., P. Wadhwani, …, A. S. Ulrich. 2009. Chemical labeling strategy with (*R*)- and (*S*)-trifluoromethylalanine for solid state ^{19}F NMR analysis of peptaibols in membranes. *J. Am. Chem. Soc.* 131: 15596–15597.

29. Glaser, R. W., C. Sachse, …, A. S. Ulrich. 2005. Concentration-dependent realignment of the antimicrobial peptide PGLa in lipid membranes observed by solid-state ^{19}F-NMR. *Biophys. J.* 88:3392–3397.

30. Bürck, J., S. Roth, …, A. S. Ulrich. 2008. Conformation and membrane orientation of amphiphilic helical peptides by oriented circular dichroism. *Biophys. J.* 95:3872–3881.

31. Wu, Y., H. W. Huang, and G. A. Olah. 1990. Method of oriented circular dichroism. *Biophys. J.* 57:797–806.

32. Olah, G. A., and H. W. Huang. 1988. Circular dichroism of oriented α-helices: I. Proof of the exciton theory. *J. Chem. Phys.* 89:2531–2538.

33. Chen, F. Y., M. T. Lee, and H. W. Huang. 2002. Sigmoidal concentration dependence of antimicrobial peptide activities: a case study on alamethicin. *Biophys. J.* 82:908–914.

34. Ellens, H., J. Bentz, and F. C. Szoka. 1984. pH-induced destabilization of phosphatidylethanolamine-containing liposomes: role of bilayer contact. *Biochemistry.* 23:1532–1538.

35. Marrink, S. J., H. J. Risselada, …, A. H. de Vries. 2007. The MARTINI force field: coarse grained model for biomolecular simulations. *J. Phys. Chem. B.* 111:7812–7824.

36. Marrink, S. J., A. H. de Vries, and A. E. Mark. 2004. Coarse grained model for semiquantitative lipid simulations. *J. Phys. Chem. B.* 108: 750–760.

37. Monticelli, L., S. K. Kandasamy, …, S.-J. Marrink. 2008. The MARTINI coarse-grained force field: extension to proteins. *J. Chem. Theory Comput.* 4:819–834.

38. Lopez, C. A., A. J. Rzepiela, …, S. J. Marrink. 2009. Martini coarse-grained force field: extension to carbohydrates. *J. Chem. Theory Comput.* 5:3195–3210.

39. Hess, B., C. Kutzner, …, E. Lindahl. 2008. GROMACS 4: algorithms for highly efficient, load-balanced, and scalable molecular simulation. *J. Chem. Theory Comput.* 4:435–447.

40. Lindahl, E., B. Hess, and D. van der Spoel. 2001. GROMACS 3.0: a package for molecular simulation and trajectory analysis. *J. Mol. Model.* 7:306–317.

41. van der Spoel, D., E. Lindahl, …, H. J. Berendsen. 2005. GROMACS: fast, flexible, and free. *J. Comput. Chem.* 26:1701–1718.

42. MARTINI. Biomolecular forcefield for coarse grained simulations. http://md.chem.rug.nl/cgmartini/. Accessed: March 31, 2012.

43. Case, D. A., T. A. Darden, …, P. A. Kollman. 2010. AMBER11. University of California, San Francisco, CA.

44. Humphrey, W., A. Dalke, and K. Schulten. 1996. VMD: visual molecular dynamics. *J. Mol. Graph.* 14:33–38, 27–28.

45. Frishman, D., and P. Argos. 1995. Knowledge-based protein secondary structure assignment. *Proteins.* 23:566–579.

46. Persistence of Vision Raytracer. http://www.povray.org: Accessed: April 1, 2012.

47. Kumar, S., D. Bouzida, …, J. Rosenberg. 1992. The weighted histogram analysis method for free-energy calculations on biomolecules. I. The method. *J. Comput. Chem.* 13:1011–1021.

48. Kumar, S., J. Rosenberg, …, P. Kollman. 1995. Multidimensional free-energy calculations using the weighted histogram analysis method. *J. Comput. Chem.* 16:1339–1350.

49. Roux, B. 1995. The calculation of the potential of mean force using computer simulations. *Comput. Phys. Commun.* 91:275–282.

50. Kelly, S. M., T. J. Jess, and N. C. Price. 2005. How to study proteins by circular dichroism. *Biochim. Biophys. Acta.* 1751:119–139.

51. Nolandt, O. V., T. H. Walther, …, A. S. Ulrich. 2009. Structure analysis of the membrane protein TatC(d) from the Tat system of *B. subtilis* by circular dichroism. *Biochim. Biophys. Acta.* 1788:2238–2244.

52. Windisch, D., S. Hoffmann, …, A. S. Ulrich. 2010. Structural role of the conserved cysteines in the dimerization of the viral transmembrane oncoprotein E5. *Biophys. J.* 99:1764–1772.

53. Abdul-Gader, A., A. J. Miles, and B. A. Wallace. 2011. A reference dataset for the analyses of membrane protein secondary structures and transmembrane residues using circular dichroism spectroscopy. *Bioinformatics.* 27:1630–1636.

54. Lobley, A., L. Whitmore, and B. A. Wallace. 2002. DICHROWEB: an interactive website for the analysis of protein secondary structure from circular dichroism spectra. *Bioinformatics.* 18:211–212.

55. Whitmore, L., and B. A. Wallace. 2004. DICHROWEB, an online server for protein secondary structure analyses from circular dichroism spectroscopic data. *Nucleic Acids Res.* 32:W668–W673.

56. Muñoz, V., and L. Serrano. 1994. Intrinsic secondary structure propensities of the amino acids, using statistical ϕ-ψ matrices: comparison with experimental scales. *Proteins.* 20:301–311.

57. Garnier, J., J. F. Gibrat, and B. Robson. 1996. GOR method for predicting protein secondary structure from amino acid sequence. *Methods Enzymol.* 266:540–553.

58. Lange, C., S. D. Müller, …, A. S. Ulrich. 2007. Structure analysis of the protein translocating channel TatA in membranes using a multiconstruct approach. *Biochim. Biophys. Acta.* 1768:2627–2634.

59. Paulmann, M., T. Arnold, …, B. Schittek. 2012. Structure-activity analysis of the dermcidin-derived peptide DCD-1L, an anionic antimicrobial peptide present in human sweat. *J. Biol. Chem.* 287:8434–8443.

60. Reference deleted in proof.

61. Huang, H. W. 2006. Molecular mechanism of antimicrobial peptides: the origin of cooperativity. *Biochim. Biophys. Acta.* 1758:1292–1302.

62. Matsuzaki, K. 1998. Magainins as paradigm for the mode of action of pore forming polypeptides. *Biochim. Biophys. Acta.* 1376:391–400.

63. Gurnev, P. A., R. Ortenberg, …, M. Bezrukov. 2011. Protective bacterial toxin TisB produces well-defined anion-selective pores in planar lipid bilayers. Biophysical Society Meeting Abstracts. *Biophys. J.* 100 (*Suppl 1*):336a.

64. Matsuzaki, K., K. Sugishita, …, K. Miyajima. 1997. Interactions of an antimicrobial peptide, magainin 2, with outer and inner membranes of Gram-negative bacteria. *Biochim. Biophys. Acta.* 1327:119–130.

65. Kandt, C., W. L. Ash, and D. P. Tieleman. 2007. Setting up and running molecular dynamics simulations of membrane proteins. *Methods.* 41: 475–488.

66. Honig, B. H., and W. L. Hubbell. 1984. Stability of "salt bridges" in membrane proteins. *Proc. Natl. Acad. Sci. USA.* 81:5412–5416.

67. Bush, J., and G. I. Makhatadze. 2011. Statistical analysis of protein structures suggests that buried ionizable residues in proteins are hydrogen bonded or form salt bridges. *Proteins.* 79:2027–2032.

68. Decoursey, T. E. 2003. Voltage-gated proton channels and other proton transfer pathways. *Physiol. Rev.* 83:475–579.

69. Reference deleted in proof.

70. Pace, C. N., F. Vajdos, …, T. Gray. 1995. How to measure and predict the molar absorption coefficient of a protein. *Protein Sci.* 4:2411–2423.

71. Johnson, W. C. 1999. Analyzing protein circular dichroism spectra for accurate secondary structures. *Proteins.* 35:307–312.

72. Sreerama, N., and R. W. Woody. 2000. Estimation of protein secondary structure from circular dichroism spectra: comparison of CONTIN, SELCON, and CDSSTR methods with an expanded reference set. *Anal. Biochem.* 287:252–260.

73. Provencher, S. W., and J. Glöckner. 1981. Estimation of globular protein secondary structure from circular dichroism. *Biochemistry.* 20:33–37.

74. van Stokkum, I. H. M., H. J. W. Spoelder, …, F. C. A. Groen. 1990. Estimation of protein secondary structure and error analysis from CD spectra. *Biochemistry.* 20:33–37.

75. Sreerama, N., and R. W. Woody. 1999. Molecular dynamics simulations of polypeptide conformations in water: a comparison of α, β, and poly(pro)II conformations. *Proteins.* 36:400–406.

76. Sreerama, N., and R. W. Woody. 1993. A self-consistent method for the analysis of protein secondary structure from circular dichroism. *Anal. Biochem.* 209:32–44.

77. Bussi, G., D. Donadio, and M. Parrinello. 2007. Canonical sampling through velocity rescaling. *J. Chem. Phys.* 126:014101.

78. Parrinello, M., and A. Rahman. 1981. Polymorphic transitions in single-crystals: a new molecular-dynamics method. *J. Appl. Phys.* 52: 7182–7190.

79. Hess, B., H. Bekker, …, J. Fraaije. 1997. LINCS: a linear constraint solver for molecular simulations. *J. Comput. Chem.* 18:1463–1472.

80. Hub, J. S., B. L. d. Groot, and D. van der Spoel. 2010. g_wham-A free weighted histogram analysis implementation including robust error and autocorrelation estimates. *J. Chem. Theory Comput.* 6:3713–3720.